

Timing and Flux Evolution of the Galactic Center Magnetar SGR J1745–2900

Victoria M. Kaspi^{1,2}, Robert F. Archibald¹, Varun Bhalerao³, François Dufour¹, Eric V. Gotthelf⁴, Hongjun An¹, Matteo Bachetti^{5,6}, Andrei M. Beloborodov⁴, Steven E. Boggs⁷, Finn E. Christensen⁸, William W. Craig^{7,9}, Brian W. Grefenstette¹⁰, Charles J. Hailey⁴, Fiona A. Harrison¹⁰, Jamie A. Kennea¹¹, Chryssa Kouveliotou¹², Kristin K. Madsen¹⁰, Kaya Mori⁴, Craig B. Markwardt¹³, Daniel Stern¹⁴, Julia K. Vogel⁹, and William W. Zhang¹³

¹*Department of Physics, McGill University, Montreal, Quebec, H3A 2T8, Canada*

²*vkaspi@physics.mcgill.ca*

³*Inter-University Center for Astronomy and Astrophysics, Post Bag 4, Ganeshkhind, Pune 411007, India*

⁴*Columbia Astrophysics Laboratory, Columbia University, New York NY 10027, USA*

⁵*Université de Toulouse, UPS-OMP, IRAP, Toulouse, France*

⁶*CNRS, Institut de Recherche en Astrophysique et Planétologie, 9 Av. colonel Roche, BP 44346, F-31028 Toulouse Cedex 4, France*

⁷*Space Sciences Laboratory, University of California, Berkeley, CA 94720, USA*

⁸*DTU Space, National Space Institute, Technical University of Denmark, Elektrovej 327, DK-2800 Lyngby, Denmark*

⁹*Lawrence Livermore National Laboratory, Livermore, CA 94550, USA*

¹⁰*Cahill Center for Astronomy and Astrophysics, California Institute of Technology, Pasadena, CA 91125, USA*

¹¹*Department of Astronomy & Astrophysics, The Pennsylvania State University, 525 Davey Lab, University Park, PA 16802, USA*

¹²*Astrophysics Office, ZP 12, NASA Marshall Space Flight Center, Huntsville, AL 35812, USA*

¹³*Goddard Space Flight Center, Greenbelt, MD 20771, USA*

¹⁴*Jet Propulsion Laboratory, California Institute of Technology, Pasadena, CA 91109, USA*

ABSTRACT

We present the X-ray timing and spectral evolution of the Galactic Center magnetar SGR J1745–2900 for the first ~ 4 months post-discovery using data obtained with the *Nuclear Spectroscopic Telescope Array (NuSTAR)* and *Swift* observatories. Our timing analysis reveals a large increase in the magnetar spin-down rate by a factor of 2.60 ± 0.07 over our data span. We further show that the change in spin evolution was likely coincident with a bright X-ray burst observed

in 2013 June by *Swift*, and if so, there was no accompanying discontinuity in the frequency. We find that the source 3–10 keV flux has declined monotonically by a factor of ~ 2 over an 80-day period post-outburst accompanied by a $\sim 20\%$ decrease in the source’s blackbody temperature, although there is evidence for both flux and kT having levelled off. We argue that the torque variations are likely to be magnetospheric in nature and will dominate over any dynamical signatures of orbital motion around Sgr A*.

Subject headings: stars: neutron — stars: magnetic field — pulsars: general — X-rays: stars

1. Introduction

The recently identified Galactic Center magnetar SGR J1745–2900 has a brief but interesting observational history. It was discovered serendipitously during an ongoing monitoring program of the Galactic Center region with the Swift X-ray Telescope (XRT). On 2013 April 24 increased X-ray emission was detected from the SGR A* region (Degenaar et al. 2013), followed the next day by a bright X-ray burst reported by Swift’s Burst Alert Telescope (BAT) (Kennea et al. 2013d,c). *Swift* XRT observations that same day refined the position of the burster to within $2.8''$ of Sgr A* (Kennea et al. 2013d). Target-of-Opportunity observations by the *Nuclear Spectroscopic Telescope Array (NuSTAR)* revealed 3.76-s pulsations from the new transient, and measured a spin-down rate that implies the presence of a neutron star having surface equatorial dipolar magnetic field strength¹ 1.6×10^{14} G (Mori et al. 2013). This identified the source as a newly outbursting magnetar in the Galactic Center (GC) region. Mori et al. (2013) also showed that the source spectrum was well described by a blackbody of $kT = 1$ keV plus a power law of index of 1.5. A *Chandra* observation later confirmed the GC association and localized the source to an offset from Sgr A* of only $2.4''$ (Rea et al. 2013). Eatough et al. (2013a) and Shannon & Johnston (2013) reported on the detection of the radio pulsar counterpart, and Eatough et al. (2013b) showed that the observed value of the rotation measure of the radio pulsar constrains the strength of the magnetic field near Sgr A*, which provides a unique test of radiative accretion theory for supermassive black holes.

Mori et al. (2013) asserted that the spin-down rate of the magnetar is sufficiently large that bias due to dynamical effects in the GC region will be negligible, unless the measured

¹Estimated assuming simple magnetic braking in a vacuum via $B = 3.2 \times 10^{19} \sqrt{P\dot{P}}$ G.

spin-down rate were temporarily greatly enhanced (e.g. due to glitch recovery; see Dib et al. 2008). Rea et al. (2013) argued dynamical effects may in principle be measurable at the $\sim 10\%$ level with long-term monitoring. However, the latter would have to be in spite of the likely continued fading of the source back to quiescence, as well as the often highly noisy nature of magnetar spin evolution post-outburst (e.g. Woods et al. 2002; Gavriil & Kaspi 2004; Dib et al. 2009; Camilo et al. 2008; Dib et al. 2012).

Also of interest, independent of the Galactic Center location, is the magnetar outburst itself. Specifically, the flux and spectral evolution of magnetars post-outburst can potentially constrain the physics of neutron star magnetospheres and/or crustal and interior composition. In the former case, magnetar outbursts are hypothesized to be due to twists in localized magnetospheric regions of enhanced current known as “j-bundles” (Beloborodov 2009). Untwisting of j-bundles involves the return of current to a hot spot on the stellar surface, with gradually decreasing luminosity and temperature, predictions that can be tested by measuring flux and spectral evolution post-outburst. In the latter case, models of crustal cooling following a sudden heat injection can be fit to magnetar cooling curves, and can constrain e.g. the depth of the energy injection as well as the nature of the stellar temperature profile (e.g. Kouveliotou et al. 2003; Scholz et al. 2012; Pons & Rea 2012; An et al. 2013). In either case, a significant hardness/flux correlation is expected and indeed thus far is generally observed (e.g. Rea & Esposito 2011; Scholz & Kaspi 2011).

Here we report on continued *NuSTAR* and *Swift* XRT monitoring of SGR J1745–2900 post-outburst, specifically its timing and flux evolution. We show that the source’s spin-down rate has recently undergone a large increase in magnitude, by over a factor of two. We suggest that the change in rate occurred coincidentally with a second X-ray burst seen by *Swift* BAT on MJD 56450 (7 June 2013) (Kennea et al. 2013a). If the burst association is correct, this change in spin-down rate occurred with no coincidental period glitch and without a large radiative change beyond the short <0.32 -s burst and possibly slightly elevated flux on that day as reported by Kennea et al. (2013a). We also report on the source’s flux and spectral evolution >100 days post-outburst.

2. Observations, Analysis and Results

The *NuSTAR* mission consists of two co-aligned focusing X-ray telescopes operating in the range 3–79 keV (Harrison et al. 2013). X-rays are focused onto CdZnTe chips (4 chips for each of two modules, A and B), yielding a point-spread function of FWHM $\sim 18''$. The *NuSTAR* detectors have 2-ms time resolution, more than adequate for studying the 3.76-s pulsar SGR J1745–2900. *NuSTAR* observed SGR J1745–2900 a total of 13 times between

MJDs 56408 (2013 April 26) and 56517 (2013 August 24) with integration times listed in Table 1.

2.1. Timing

For timing purposes, for each *NuSTAR* observation, we extracted photons in a $1'$ radius around the nominal source position using the *NuSTAR Data Analysis Software (NuSTAR-DAS)* version 1.2.0, along with HEASOFT version 6.13. The data were reduced to the Solar System barycenter assuming the *Chandra* position reported by Rea et al. (2013) and the DE200 planetary ephemeris. We also filtered the data to extract only photons with energies 3–10 keV, as this generally provided an optimal signal-to-noise strength on the pulse. Average pulse times-of-arrival (TOAs) were extracted from the event lists by first folding the X-ray time series at the nominal pulse period and then aligning the resulting profile with a high signal-to-noise ratio template in the Fourier domain taking into account 6 Fourier harmonics, although our results are not strongly dependent on this choice. We have observed the pulse profile to be largely stable long-term, apart from the slow disappearance of the first peak seen in Figure 1 of Mori et al. (2013); see our Figure 1. This gives us confidence in the reliability of the TOA extraction method as the primary and third peaks have remained unchanged. The resulting TOAs were then fed into the `tempo` software package² for further analysis. Note that we have verified that *NuSTAR*'s clock is sufficiently stable (i.e. reliable in absolute timing to well under 10 ms on comparable time scales to those considered here) that it contributes negligibly to the uncertainties in the TOAs.

We further supplemented the *NuSTAR* TOAs with timing data extracted from *Swift* XRT (Burrows et al. 2005) Windowed Timing (WT) observations of the source. Photon-counting mode data could not be included as they had insufficient timing resolution. To produce the *Swift* TOAs, Level 1 data products were obtained from the HEASARC *Swift* archive and reduced using the *xrtpipeline* standard reduction in HEASOFT version 6.13. We extracted photons in a $47''$ radius around the nominal source position, and reduced the resulting event times to the Solar System barycentre. The *Swift* data were also filtered to include only photons from 3–10 keV. The resulting events were then subjected to the same TOA extraction analysis as for the *NuSTAR* data. The details of the *Swift* observations are presented in Table 1. Note that one WT-mode observation (ObsID 00032811004 on MJD 56429) was omitted from the analysis due to poor statistics.

The ephemeris reported by Mori et al. (2013) provided an excellent fit to the initial

²<http://www.atnf.csiro.au/research/pulsar/tempo/>

NuSTAR data, and we further refine it here with subsequent observations. Our best-fit parameters for this first ephemeris are presented in Table 2. However TOAs added from observations made on MJDs 56439 and 56457 deviated significantly by ~ 0.1 from the prediction of an ephemeris fit using all earlier data. This deviation alone is not large enough to rule out extrapolation of this ephemeris to those epochs, as their phase deviation could be mostly fit out using a large second frequency derivative. By MJD 56480, however, this first ephemeris clearly described the phase data poorly, precluding proper phase counting, even with a second derivative.

We therefore initiated a series of closely spaced observations in order to reacquire phase lock. This resulted in a second phase-coherent ephemeris with significantly different spin-down rate, as shown in Table 2; the featureless residuals from this new ephemeris are shown in Figure 2. The backward extrapolation of this second ephemeris to MJDs 56457 and 56439 also showed a significant phase deviation, however again a (new) second frequency derivative could reasonably be fit to remove the deviation. Backward extrapolation of the new ephemeris beyond those epochs resulted in significant phase wraps, as shown in Figure 3, even with this new second derivative.

The two coherent ephemerides are plotted in solid lines in Figure 4. There the overlap region between MJDs 56439 and 56457 is shown and the difference between the two ephemerides is clear. To determine which ephemeris better fits the data in the overlap region, we fit local frequencies to the TOAs at those epochs, as the *NuSTAR* integration times were sufficiently long to allow this measurement. The resulting frequencies are plotted in solid circles, with `tempo`-reported 1σ uncertainties shown. Clearly the frequency from the MJD 56439 observation is inconsistent with the second ephemeris, indicating those data are best described by the first ephemeris.

In Figure 4 we plot in red the epochs of the three X-ray bursts reported by *Swift* BAT (Kennea et al. 2013d,a,b). Interestingly, the second burst coincided within uncertainties to the epoch at which our two ephemerides converge; specifically, at the observed burst epoch (11:17:26 UT on June 7, 2013, or MJD 56450.47044), the extrapolated frequencies of the two ephemerides agree at the 1.9σ level. This suggests that the burst likely coincided with the change in spin-down rate, if indeed the change was abrupt. It further suggests that the burst event occurred with no frequency discontinuity, i.e. with no spin-up or spin-down glitch. We set a 3σ upper limit on the amplitude of such a glitch, assuming it coincided with the BAT burst, of $\Delta\nu/\nu < 1.1 \times 10^{-6}$. This upper limit is in the mid-range of observed fractional frequency changes in magnetar bursts (Kaspi et al. 2003; Dib et al. 2008, 2009, e.g.). If, in fact, the burst was not coincident with the ephemeris change, then the latter accompanied a spin-up glitch if it preceded the burst, and a spin-down glitch if it followed.

On the other hand, the change in ephemeris may have been gradual and with no frequency discontinuity; in that case, however, that the burst epoch coincided with the convergence of the two independently determined ephemerides would have to be merely luck.

2.2. Flux and Spectroscopy

2.2.1. *Swift* Observations

First, to consider the overall soft-band flux evolution of the source, we analyzed Photon Counting mode data from *Swift* XRT. Specifically, we include 109 PC-mode observations obtained between MJDs 56407 and 56550. For this work we did not use WT-mode data as they suffered from very high background and were not informative, but we verified they were broadly consistent with the PC mode results. To extract the *Swift* fluxes, we obtained Level 1 data products from the HEASARC *Swift* archive and reduced them using the xrtpipeline standard reduction in HEASOFT, using grade 0 data, and including an exposure map. The selected source region is a circle with 20'' radius centered at the *Chandra* position for SGR J1745–2900. This radius was selected as it approximates the *Swift* XRT half-power diameter at 4 keV (Moretti et al. 2005). A source-free background region of the same size was selected in a nearby region. Observations were typically 1-ks long, and occurred nearly daily. Spectra from the observations were summed in 5-day intervals and the results grouped with a minimum of 3 counts per spectral bin. Spectra were fit using the ‘lstat’ statistic, and absorption modelled using Wilms et al. (2000) abundances and Verner et al. (1996) cross sections. Fluxes measured between MJD 56430-35 were contaminated by a transient source (Transient 1; see §2.2.2) so were omitted from the analysis. The spectra were fit linking N_H as well as kT , as this was statistically preferred, i.e. a variable kT did not improve the quality of the fit significantly, given the available statistics. In this way, we found best-fit values of $N_H = 15.3_{-0.6}^{+0.7} \times 10^{22} \text{ cm}^{-2}$ and $kT = 0.94 \pm 0.02 \text{ keV}$. These value are consistent with the results of Mori et al. (2013) as well as with those from *Chandra* (Rea et al. 2013). The flux evolution that results from these fits is shown in Figure 4.

2.2.2. *NuSTAR* Observations

The analysis of the *NuSTAR* spectral data for SGR J1745–2900 required particular care because two nearby transient sources impacted the data at different times. These transients are CXOGC J174540.0–290005, 24'' from the magnetar (henceforth Transient 1; see ATELS 5095, 5074) and AX J1745.6–2901, 88'' away (henceforth Transient 2; see ATELS

5226, 1513). Both transients are Low Mass X-ray Binaries (LMXBs) and contaminated the *NuSTAR* magnetar spectral data significantly; the contamination was so severe we ignored the spectral data in the epochs when Transient 1 was bright (MJDs 56430, 56439), and processed with great caution when Transient 2 was bright (MJDs 56504, 56512, 56513, 56517). Stray light from an unrelated source also contaminated the background in Module B for one observation; see Table 1. Data were processed using `nupipeline` and `nuproducts` from the public release with `HEASOFT` 6.14. The extraction region was selected as a circle of 30'' radius centered on the source position. Response matrices appropriate for each data set were also generated using the standard software. In our spectral fitting, for interstellar X-ray absorption modelling, we assumed Wilms et al. (2000) abundances and Verner et al. (1996) cross sections. We considered only the energy range 3–30 keV, as the source was not detected at higher energies in any observation.

The Galactic Center region is crowded and the background is spatially variable. Moreover, the unrelated transients affected the data significantly. As a result, extracting a separate background region for the magnetar was in general not feasible. In order to evaluate the robustness of our results, we used two different, independent methods to analyse these data. The first method subtracted background spectra obtained from pre-outburst data, while the second modelled the background spectra along with the magnetar’s. For all the observations under consideration, in the source extraction region around the magnetar and in the energy band we analyzed (3–30 keV), Galactic center diffuse emission dominated while the internal and stray-light backgrounds were negligible. Both of our methods described below are appropriate when the background is dominant. As we show, the two methods largely agree, implying our reported results are robust.

In Method 1, we selected one of the pre-outburst images of the field (ObsID 30001002003 taken on MJD 56413) as our background exposure. The integration time for this observation was much longer than in any of the magnetar exposures, so the uncertainties in fit parameters are dominated by source statistics. We have verified that the off-axis angle of the source (and pre-outburst background) was similar for all epochs so that variations in the ARF between source and background regions are small (under $\sim 5\%$).

The *NuSTAR* spectra are plotted in Figure 5. We tested various spectral models for the magnetar, using `XSEPC` version 12.8.1. We binned the spectra to have a minimum of 20 counts per spectral bin and used χ^2 statistics in this method. Physically, we do not expect the column density N_H towards this source to vary on the relevant time scales, hence we fit jointly for N_H across all observations using the `tbabs` function in `XSPEC`. The best fit was obtained by the conventionally used empirical two-component model consisting of an absorbed blackbody plus power law, with overall reduced $\chi^2_\nu = 1.03$ for 3683 degrees of freedom.

Our best-fit fluxes and blackbody temperatures and radii (calculated assuming a distance of 8.0 kpc) are shown in Figure 6. Fits with just one spectral component were significantly worse. Although initially we allowed the blackbody and power-law model parameters to vary, we also tried fitting the models assuming a constant power-law index. The resulting fits, with constant and variable power-law index, are of similar quality, and yield similar results for the blackbody component. The best-fit value obtained for N_H , $(13.5 \pm 0.5) \times 10^{22} \text{ cm}^{-2}$, was consistent with the values reported by Mori et al. (2013) and Rea et al. (2013). The best-fit value of the assumed constant fit power-law index was 1.43 ± 0.15 . The best-fit kT values and effective radii are plotted in Figure 6. The χ^2 value for the overall fit was 6722 for 6425 degrees of freedom. We note that our need for a power-law component, even a constant value as a minimum, is consistent with the hint of high-energy excess reported by Rea et al. (2013) from *Chandra* data.

Given that Transient 2 is ~ 10 times brighter than the magnetar and that their PSFs overlap, our method for handling the data affected by Transient 2 requires a special description. Transient 2 was extracted and reduced in a similar fashion to the magnetar itself, but was fit with an absorbed blackbody plus disk model, based on similar fits done to this source in the past (Hyodo et al. 2009). The contamination of Transient counts within the magnetar extraction region was then estimated using the PSF file from *NuSTAR*'s CALDB; we concluded 0.035 of the transient's total flux fell within our magnetar extraction region in our energy range, which amounted to roughly half of the magnetar's flux in its aperture. We then fit the spectra of both objects jointly but tying the Transient's parameters, and ignoring the magnetar's flux within the Transient's extraction region. Allowing the contamination factor to vary gave similar results, and the best-fit contamination factor was close to the calculated one. Note that we did not detect the source above 10 keV in the last four *NuSTAR* observations so for those epochs 99% confidence upper limits are presented in the 10–30 keV energy range. For all other observations, the detection significances in the 10–30 keV band ranged from 10.4σ (at the start of the observations) to 5.6σ (at the last observation for which there was a significant detection in this band).

In spectral analysis Method 2, we selected a background region for each observation that included all of the chip on which the source region falls, but excluded two bright features (Sgr A* and the Sgr A-E knot), as observed in a mosaic of all observations of the field in which no transient was present, as well as stray light patterns from nearby bright sources. In individual observations, we found the selected background to always be subdominant compared to the source spectrum in our energy range. In this Method, we used **XSPEC** v.12.8.0m, binned the spectra by a minimum of 3 counts per bin, and used the 'lstat' fitting statistic.

We first fit a spectral model to the diffuse emission in the background regions. We jointly

fit all the background regions, using two velocity-broadened APEC thermal plasma models (`bapec` in `XSPEC`) plus a power-law component, with photoelectric absorption. The velocity broadening of both plasma models was linked, as were all diffuse emission parameters for all observations, except the overall normalization, which was allowed to vary between modules A and B. We fit the diffuse emission in observations where the magnetar is absent, and found a reasonable model with featureless residuals throughout the fitted band. This demonstrated to us that our background model is reasonable as a phenomenological description sufficient for our purposes. For a more physically relevant consideration of the background spectrum in this energy band, see Krivonos et al. (2013).

We then fitted each magnetar observation individually using this independently determined diffuse emission model with variable parameters as background. For the magnetar’s spectrum, we assumed a model consisting of a blackbody plus power law, photoelectrically absorbed. We used a Markov-Chain Monte Carlo method to explore the likelihood landscape of a joint fit to all the data. The absorption column of the magnetar’s spectral model was linked for all observations but the normalization was allowed to vary between modules (though linked for each module between all observations), with all other parameters left free to vary between observations (but linked for both modules of the same observation). Fitted power-law indexes were poorly constrained. When linking the magnetar’s power-law index across all observations, we found this to be slightly statistically disfavored but the impact on the kT values not significant. Data contaminated by Transient 2 are not reported for Method 2 as for these we could not find stable results.

The results of our *NuSTAR* spectral analysis for the magnetar for both Methods are summarized in Figure 6. In the Figure, we show in the top two panels the flux evolution with time in two bands, 3–10 keV and 10–30 keV. Note the difference in scale between the two in the Figure. The results are qualitatively the same for Methods 1 and 2: the soft band flux decreases monotonically, quasi-linearly, by a factor of ~ 2 over 80 days, while the hard band flux shows greater variation – notably an increase at the fourth epoch 23 days post-outburst, and a greater decrease subsequently such that by 80 days post-outburst, it is a factor of ~ 4 lower than in our initial observation. In panel (c) we plot a hardness ratio, defined as the ratio of the flux in the 10–30 keV band to that in the 3–10 keV band. Methods 1 and 2 show good qualitative and near-quantitative agreement: the source indeed hardens significantly at the fourth epoch. The third panel from the top shows the evolution of blackbody temperature kT . There is clear evidence for a decrease in kT with time, at least until 60 days post-outburst, in spite of the apparent increase in 10–30 keV flux at 23 days. The bottom panel shows blackbody radius evolution assuming a distance to the magnetar of 8.0 kpc. Here we find our Methods disagree somewhat at the fourth and fifth epochs; regardless, overall it is clear that the blackbody radius remained nearly constant overall, to

at least within 30–40%.

The *Swift* spectral results described in §2.2.1 are consistent with those of *NuSTAR* in the 3–10 keV band, as shown in Figure 6, although we note a normalization offset. This may be a result of cross-calibration uncertainties or due to imperfect background subtraction, as we found the normalization of the *Swift* fluxes depended significantly on the exact location of the selected background region.

3. Discussion

3.1. Spin Evolution

The coincidence of the second BAT burst with the intersection of the first and second ephemerides, as shown graphically in Figure 4, is striking. If not due to chance, the spin-down rate of the magnetar changed abruptly at the burst epoch and there was no frequency discontinuity of any type, either a spin-up or spin-down glitch, at that epoch.

Regardless of exactly how the change in spin-down rate occurred, we have shown that its magnitude has increased. Comparing extrapolated values of $\dot{\nu}$ at the start of our observations (MJD 56408) with that at the end (MJD 56519), we show that its magnitude has changed by a factor of 2.60 ± 0.07 , that is, has nearly tripled in less than 4 months. Moreover, the magnitude is continuing to increase.

Large torque variations have been seen ubiquitously in magnetars (e.g. Woods et al. 2002; Kaspi et al. 2003; Gavriil & Kaspi 2004; Camilo et al. 2007, 2008; Dib et al. 2012; Archibald et al. 2013; Dib & Kaspi 2013). These torque variations can be categorized in two main classes: (i) those following glitches; and (ii) those unassociated with glitches. The former can be seen immediately after a spin-up or spin-down event and are generally similar to the recoveries seen post-glitch in many radio pulsars (e.g. Yuan et al. 2010; Espinoza et al. 2011; Yu et al. 2013). These recoveries are thought to be related to repinning of angular momentum vortices in the superfluid component of the stellar crust after a major unpinning event (Alpar et al. 1984, 2000, 1993), although in the context of magnetars, scenarios involving the magnetosphere have also been suggested (e.g. Parfrey et al. 2012, 2013; Lyutikov 2013). Thompson et al. (2000) discussed these possibilities in the context of torque variations comparable to that seen in SGR J1745–2900 but observed in SGR 1900+14 following its 1998 giant flare. However, since we find evidence for a glitch in SGR J1745–2900, glitch-specific models do not seem relevant here.

Thompson et al. (2000) proposed torque variations unassociated with glitches could

arise due to particle outflow. In this picture, the energy output observed in the giant flare of SGR 1900+14 was insufficient to explain the torque change; Thompson et al. (2000) required a radiation-hydrodynamical outflow of even higher energy output. As no giant flare has been observed from SGR J1745–2900, this model does not seem to apply here.

Magnetar torque variations have also been suggested to be purely magnetospheric in origin (e.g. Beloborodov 2009). In general, a burst signals a sudden re-arrangement of a part of the magnetosphere. If this part involves the open field lines, the spin-down torque must change. Note that the open magnetic flux is a tiny fraction $\sim 10^{-4}$ of the total magnetic flux of the star, so the spin-down torque is sensitive to the behavior of a tiny fraction of the magnetosphere. In the context of the scenario proposed by Beloborodov (2009), the persistent luminosity is produced by a much more energetic closed j-bundle which may or may not contain the open flux. If a burst affects the open flux but does not affect the j-bundle much, the torque can change while the X-ray luminosity does not, as is observed here, since near the second burst epoch where the torque seems to have begun to change, there is no feature in the source’s flux evolution beyond the continued decay following the source’s initial appearance in 2013 April. Indeed we find it interesting that at the second burst epoch, no glitch was seen *and* no flux change was detected (apart from the brief burst itself and the continued decay following the source’s initial appearance). It could be that in magnetar outbursts, part of the observed enhanced flux results from the interior of the star and originates from heat released in an internal glitch, whereas another component of the enhanced flux originates from purely magnetospheric processes. This could explain why, for example, in the 2002 outburst of magnetar 1E 2259+586, there were two clearly different time scales associated with the decay of the initial flux enhancement: one very short, on a 1–2-day time scale, and one lasting months (Woods et al. 2004; Zhu et al. 2008). Perhaps the short-term X-ray flux enhancement and decay is a result of transient glitch-related emission, whereas the much longer decay is due to magnetospheric untwisting and/or crustal cooling.

Regardless of the origin of the torque variations, they clearly will dominate over dynamical effects due to the orbit around Sgr A*. Rea et al. (2013) have argued that variations in the spin-down rate as large as 10% due to acceleration in the field of Sgr A* might one day be observed, however, the observations reported here demonstrate that the spin evolution of this magnetar, like those of many others, is inherently unstable and unlikely to permit such a measurement. The discovery of a rotation-powered pulsar, particularly a millisecond radio pulsar, in similar proximity to Sgr A*, would be far more useful for dynamical studies of the black hole environment.

3.2. Spectral Evolution

We have shown that the 3–10 keV flux of SGR J1745–2900 has declined since the source’s initial appearance, albeit rather slowly, only by a factor of ~ 2 over the first 80 days since the discovery outburst. This is similar to what was found by Rea et al. (2013) on the basis of three *Chandra* observations. The flux decay on a timescale of $\sim 10^7$ s was predicted by Mori et al. (2013) based on the observed emission area of the blackbody component, A , and the untwisting magnetosphere model of Beloborodov (2009). Specifically, Mori et al. (2013) estimated a luminosity evolution time scale of $t_{ev} \simeq 10^7 \mu_{32} \Phi_{10}^{-1} A_{11.5}$ s, where μ_{32} is the magnetic moment in units of 10^{32} G cm³, Φ_{10}^{-1} is the electric voltage sustaining e^\pm discharge in the magnetosphere in units of 10^{10} V, and $A_{11.5}$ is in units of $10^{11.5}$ cm². This predicted time scale is roughly consistent with the flux decay we report. The model also predicts that the hot spot should shrink, approximately as $A \propto L_{BB}^{1/2}$, where L_{BB} is the blackbody luminosity. When L_{BB} decreases by a factor of 2, area A is expected to decrease by $\sim 40\%$ and the blackbody radius by $\sim 20\%$. There may be a hint of such a radius decrease in the bottom panel of Figure 4, but given the contamination due to Transient 2, our observations cannot confirm this.

The blackbody temperature also decreased monotonically by $\sim 20\%$ over the first 60-days post-outburst, although as is clear in Figure 5, there is a possible hint of an increase in the subsequent *NuSTAR* observation at 80 days. Due to the presence of Transient 2, we cannot verify unambiguously whether this trend continued, since our subsequent observations may be contaminated and the *Swift* XRT observations yield insufficient statistics to detect such a change. *Chandra* observations, given that telescope’s superior angular resolution that should preclude the transient source contamination, may be able to address this question. Meanwhile, however, we note with interest the apparent hardening of the magnetar’s flux in our fourth observation 23 days post-outburst (see Fig. 5); this was unaccompanied by any significant frequency or torque change, nor by any observed burst. This is puzzling and could indicate a burst that went unseen by all-sky monitors just prior, or perhaps it could be due to a different source appearing within the *NuSTAR* PSF. Regardless, we have not observed the common magnetar flux/hardness correlation (e.g. Woods et al. 2004; Gotthelf & Halpern 2007; Zhu et al. 2008; Tam et al. 2008; Rea & Esposito 2011; Scholz & Kaspi 2011) in this source; this may be due to the relatively small range of fluxes yet observed, although we note no clear correlation was seen for SGR 1627–41 either, for a much larger flux range (An et al. 2012). Given the typical behavior of other magnetars, we expect the source spectrum to gradually soften as the flux continues to decline, although presently, both flux and temperature show evidence for leveling off. We further note the relative stability of the inferred effective blackbody radius (Fig. 4); any model to explain the flux decline will also have to account for a relatively stable emitting area. Some crustal cooling models predict an

increase in emitting area as the initially localized internal heat spreads around the neutron-star surface, while relaxation following a magnetospheric twist as discussed above should involve a decrease in the emitting region, the footpoint of the j-bundle (Beloborodov 2009). Continued observations of the source spectrum as the emission fades may help distinguish between these two possible processes in the star.

4. Conclusions

We have reported on X-ray observations made by *NuSTAR* and *Swift* over ~ 120 days after the initial outburst of the Galactic Center magnetar SGR J1745–2900 in 2013 April. We find that the magnetar’s spin-down torque has increased by a factor of nearly 3 compared with the spin-down rate initially measured by Mori et al. (2013), with no evidence for any accompanying spin-up or spin-down glitch. We also show that the pulsar’s 3–10 keV flux has declined monotonically by a factor of ~ 2 over the first post-outburst 80 days, and that the blackbody temperature has decreased by $\sim 20\%$ over the initial 60 days, similar to what was reported by Rea et al. (2013), although we find evidence for a possible levelling-off of both flux and temperature. We observed a likely increase in the source’s 10–30 keV flux 17 days post-outburst, but observe no accompanying timing or burst event. We find no evidence for the hardness/flux correlation commonly observed in magnetars, although this seems likely due to the narrow range of fluxes we have yet sampled. Further monitoring may yet reveal spectral softening as the source flux declines. We argue that the origin of the increase in the spin-down rate is likely to be magnetospheric, and that such torque variations, ubiquitous in magnetars, are likely to dominate over any timing signatures of motions related to the magnetar’s proximity to Sgr A*.

This work was supported under NASA Contract No. NNG08FD60C, and made use of data from the *NuSTAR* mission, a project led by the California Institute of Technology, managed by the Jet Propulsion Laboratory, and funded by the National Aeronautics and Space Administration. We thank the *NuSTAR* Operations, Software and Calibration teams for support with the execution and analysis of these observations. This research has made use of the *NuSTAR* Data Analysis Software (NuSTARDAS) jointly developed by the ASI Science Data Center (ASDC, Italy) and the California Institute of Technology (USA). We acknowledge the use of public data from the Swift data archive. This research has made use of the XRT Data Analysis Software (XRTDAS) developed under the responsibility of the ASI Science Data Center (ASDC), Italy. We thank the *Swift* SOT team for their work in scheduling. VMK receives support from an NSERC Discovery Grant and Accelerator Supplement, from the Centre de Recherche en Astrophysique du Québec, an R. Howard

Webster Foundation Fellowship from the Canadian Institute for Advanced Study, the Canada Research Chairs Program and the Lorne Trottier Chair in Astrophysics and Cosmology. RFA receives support from a Walter C. Sumner Memorial Fellowship. AMB was supported by NASA grants NNX-10-AI72G and NNX-13-AI34G. JAK was supported by supported by NASA contract NAS5-00136. JKV's work was performed under the auspices of the U.S. Department of Energy by Lawrence Livermore National Laboratory under Contract DE-AC52-07NA27344.

REFERENCES

- Alpar, M. A., Anderson, P. W., Pines, D., & Shaham, J. 1984, *ApJ*, 276, 325
- Alpar, M. A., Chau, H. F., Cheng, K. S., & Pines, D. 1993, *ApJ*, 409, 345
- Alpar, M. A., Pines, D., & Cheng, K. S. 2000, *Nature*, 348, 707
- An, H., Kaspi, V. M., Archibald, R., & Cumming, A. 2013, *ApJ*, 763, 82
- An, H., Kaspi, V. M., Tomsick, J. A., Cumming, A., Bodaghee, A., Gotthelf, E. V., & Rahoui, F. 2012, *ApJ*, 757, 68
- Archibald, R. F., Kaspi, V. M., Ng, C.-Y., Gourgouliatos, K. N., Tsang, D., Scholz, P., Beardmore, A. P., Gehrels, N., & Kennea, J. A. 2013, *Nature*, 497, 591
- Beloborodov, A. M. 2009, *ApJ*, 703, 1044
- Burrows, D. N., Hill, J. E., Nousek, J. A., Kennea, J. A., Wells, A., Osborne, J. P., Abbey, A. F., Beardmore, A., Mukerjee, K., Short, A. D. T., Chincarini, G., Campana, S., Citterio, O., Moretti, A., Pagani, C., Tagliaferri, G., Giommi, P., Capalbi, M., Tamburelli, F., Angelini, L., Cusumano, G., Bräuninger, H. W., Burkert, W., & Hartner, G. D. 2005, *Space Sci. Rev.*, 120, 165
- Camilo, F., Cognard, I., Ransom, S. M., Halpern, J. P., Reynolds, J., Zimmerman, N., Gotthelf, E. V., Helfand, D. J., Demorest, P., Theureau, G., & Backer, D. C. 2007, *ApJ*, 663, 497
- Camilo, F., Reynolds, J., Johnston, S., Halpern, J. P., & Ransom, S. M. 2008, *ApJ*, 679, 681
- Degenaar, N., Reynolds, M. T., Miller, J. M., Kennea, J. A., & Wijnands, R. 2013, *The Astronomer's Telegram*, 5006

- Degenaar, N., Wijnands, R., Reynolds, M. T., Miller, J. M., Kennea, J. A., & Gehrels, N. 2013, *The Astronomer’s Telegram*, 5074
- Dib, R. & Kaspi, V. M. 2013, *ApJS*
- Dib, R., Kaspi, V. M., & Gavriil, F. P. 2008, *ApJ*, 673, 1044
- . 2009, *ApJ*, 702, 614
- Dib, R., Kaspi, V. M., Scholz, P., & Gavriil, F. P. 2012, *ApJ*, 748, 3
- Dufour, F., Kaspi, V. M., Gotthelf, E. V., Baganoff, F. K., & Harrison, F. A. 2013, *The Astronomer’s Telegram*, 5073
- Eatough, R., Karuppusamy, R., Kramer, M., Klein, B., Champion, D., Kraus, A., Keane, E., Bassa, C., Lyne, A., Lazarus, P., Verbiest, J., Freire, P., Brunthaler, A., & Falcke, H. 2013a, *The Astronomer’s Telegram*, 5040
- Eatough, R. P., Falcke, H., Karuppusamy, R., Lee, K. J., Champion, D. J., Keane, E. F., Desvignes, G., Schnitzeler, D. H. F. M., Spitler, L. G., Kramer, M., Klein, B., Bassa, C., Bower, G. C., Brunthaler, A., Cognard, I., Deller, A. T., Demorest, P. B., Freire, P. C. C., Kraus, A., Lyne, A. G., Noutsos, A., Stappers, B., & Wex, N. 2013b, *nature*
- Espinoza, C. M., Lyne, A. G., Stappers, B. W., & Kramer, M. 2011, *MNRAS*, 414, 1679
- Gavriil, F. P. & Kaspi, V. M. 2004, *ApJ*, 609, L67
- Gotthelf, E. V. & Halpern, J. P. 2007, *ApJ*, 664, L35
- Harrison, F. A., Craig, W. W., Christensen, F. E., Hailey, C. J., Zhang, W. W., Boggs, S. E., Stern, D., Cook, W. R., Forster, K., Giommi, P., Grefenstette, B. W., Kim, Y., Kitaguchi, T., Koglin, J. E., Madsen, K. K., Mao, P. H., Miyasaka, H., Mori, K., Perri, M., Pivovarov, M. J., Puccetti, S., Rana, V. R., Westergaard, N. J., Willis, J., Zoglauer, A., An, H., Bachetti, M., Barrière, N. M., Bellm, E. C., Bhalerao, V., Brejnholt, N. F., Fuerst, F., Liebe, C. C., Markwardt, C. B., Nynka, M., Vogel, J. K., Walton, D. J., Wik, D. R., Alexander, D. M., Cominsky, L. R., Hornschemeier, A. E., Hornstrup, A., Kaspi, V. M., Madejski, G. M., Matt, G., Molendi, S., Smith, D. M., Tomsick, J. A., Ajello, M., Ballantyne, D. R., Baloković, M., Barret, D., Bauer, F. E., Blandford, R. D., Brandt, W. N., Brenneman, L. W., Chiang, J., Chakrabarty, D., Chenevez, J., Comastri, A., Dufour, F., Elvis, M., Fabian, A. C., Farrah, D., Fryer, C. L., Gotthelf, E. V., Grindlay, J. E., Helfand, D. J., Krivonos, R., Meier, D. L., Miller, J. M., Natalucci, L., Ogle, P., Ofek, E. O., Ptak, A., Reynolds, S. P., Rigby, J. R., Tagliaferri, G., Thorsett, S. E., Treister, E., & Urry, C. M. 2013, *ApJ*, 770, 103

- Hyodo, Y., Ueda, Y., Yuasa, T., Maeda, Y., Makishima, K., & Koyama, K. 2009, PASJ, 61, 99
- Kaspi, V. M., Gavriil, F. P., Woods, P. M., Jensen, J. B., Roberts, M. S. E., & Chakrabarty, D. 2003, ApJ, 588, L93
- Kennea, J. A., Burrows, D. N., Cummings, J., Kouveliotou, C., Degenaar, N., Reynolds, M. T., Miller, J. M., & Wijnands, R. 2013a, The Astronomer’s Telegram, 5124
- Kennea, J. A., Burrows, D. N., Cummings, J., Krimm, H. A., Barthelmy, S., Kouveliotou, C., Degenaar, N., Reynolds, M. T., Miller, J. M., & Wijnands, R. 2013b, The Astronomer’s Telegram, 5254
- Kennea, J. A., Burrows, D. N., Kouveliotou, C., Palmer, D. M., Göğüş, E., Kaneko, Y., Evans, P. A., Degenaar, N., Reynolds, M. T., Miller, J. M., Wijnands, R., Mori, K., & Gehrels, N. 2013c, ApJ, 770, L24
- Kennea, J. A., Krimm, H., Barthelmy, S., Gehrels, N., Markwardt, C., Cummings, J., Marshall, F., Sakamoto, T., Degenaar, N., Reynolds, M. T., Miller, J. M., & Kouveliotou, C. 2013d, The Astronomer’s Telegram, 5009
- Kouveliotou, C., Eichler, D., Woods, P. M., Lyubarsky, Y., Patel, S. K., Göğüş, E., van der Klis, M., Tennant, A., Wachter, S., & Hurley, K. 2003, ApJ, 596, L79
- Krivonos, R. A., Tomsick, J. A., Bauer, F. E., Baganoff, F. K., Barriere, N. M., Bodaghee, A., Boggs, S. E., Christensen, F. E., Craig, W. W., Grefenstette, B. W., Hailey, C. J., Harrison, F. A., Hong, J., Madsen, K. K., Mori, K., Nynka, M., Stern, D., & Zhang, W. W. 2013, ApJ, in press
- Lyutikov, M. 2013, ArXiv e-prints
- Mori, K., Gotthelf, E. V., Zhang, S., An, H., Baganoff, F. K., Barrière, N. M., Beloborodov, A. M., Boggs, S. E., Christensen, F. E., Craig, W. W., Dufour, F., Grefenstette, B. W., Hailey, C. J., Harrison, F. A., Hong, J., Kaspi, V. M., Kennea, J. A., Madsen, K. K., Markwardt, C. B., Nynka, M., Stern, D., Tomsick, J. A., & Zhang, W. W. 2013, ApJ, 770, L23
- Parfrey, K., Beloborodov, A. M., & Hui, L. 2012, ApJ, 754, L12
- . 2013, ApJ, 774, 92
- Rea, N. & Pons, J. 2012, ApJ, 750, L6

- Rea, N. & Esposito, P. 2011, in *High-Energy Emission from Pulsars and their Systems*, ed. D. F. Torres & N. Rea (Springer-Verlag), 247
- Rea, N., Esposito, P., Pons, J. A., Turolla, R., Torres, D. F., Israel, G. L., Possenti, A., Burgay, M., Viganò, D., Perna, R., Stella, L., Ponti, G., Baganoff, F., Haggard, D., Papitto, A., Camero-Arranz, A., Zane, S., Minter, A., Mereghetti, S., Tiengo, A., Schoedel, R., Feroci, M., Mignani, R., & Gotz, D. 2013, ArXiv e-prints
- Scholz, P. & Kaspi, V. M. 2011, *ApJ*, 739, 94
- Scholz, P., Ng, C.-Y., Livingstone, M. A., Kaspi, V. M., Cumming, A., & Archibald, R. F. 2012, *ApJ*, 761, 66
- Shannon, R. M. & Johnston, S. 2013, *MNRAS*
- Tam, C. R., Gavriil, F. P., Dib, R., Kaspi, V. M., Woods, P. M., & Bassa, C. 2008, *ApJ*, 677, 503
- Thompson, C., Duncan, R. C., Woods, P. M., Kouveliotou, C., Finger, M. H., & van Paradijs, J. 2000, *ApJ*, 543, 340
- Verner, D. A., Ferland, G. J., Korista, K. T., & Yakovlev, D. G. 1996, *ApJ*, 465, 487
- Wilms, J., Allen, A., & McCray, R. 2000, *ApJ*, 542, 914
- Woods, P. M., Kaspi, V. M., Thompson, C., Gavriil, F. P., Marshall, H. L., Chakrabarty, D., Flanagan, K., Heyl, J., & Hernquist, L. 2004, *ApJ*, 605, 378
- Woods, P. M., Kouveliotou, C., Göğüş, E., Finger, M. H., Swank, J., Markwardt, C. B., Hurley, K., & van der Klis, M. 2002, *ApJ*, 576, 381
- Yu, M., Manchester, R. N., Hobbs, G., Johnston, S., Kaspi, V. M., Keith, M., Lyne, A. G., Qiao, G. J., Ravi, V., Sarkissian, J. M., Shannon, R., & Xu, R. X. 2013, *MNRAS*, 429, 688
- Yuan, J. P., Manchester, R. N., Wang, N., Zhou, X., Liu, Z. Y., & Gao, Z. F. 2010, *ApJ*, 719, L111
- Zhu, W., Kaspi, V. M., Dib, R., Woods, P. M., Gavriil, F. P., & Archibald, A. M. 2008, *ApJ*, 686, 520

Table 1: Timing Observations of SGR J1745–2900

Obs. ID	Date	MJD ^a	T_{int} (ks)	Contamination ^b
<i>NuSTAR</i>				
30001002006	04/26/2013	56408	37.2	
80002013002	04/27/2013	56409	49.8	
80002013004	05/04/2013	56416	38.6	
80002013006	05/11/2013	56423	32.7	
80002013008	05/18/2013	56430	39.0	T1
80002013010	05/27/2013	56439	37.4	T1
80002013012	06/14/2013	56457	26.7	
80002013014/6	07/07/2013	56480	29.5 ^c	
80002013018	07/31/2013	56504	22.3	T2
80002013020	08/08/2013	56512	12.0	T2
80002013022	08/09/2013	56513	11.2	T2
80002013024	08/13/2013	56517	11.7	T2
<i>Swift</i>				
00032811001	05/03/2013	56415	15.5	
00032811002	05/11/2013	56423	9.2	
00032811003	05/16/2013	56428	9.5	
00032811005	05/19/2013	56431	13.5	
00032811006	06/07/2013	56450	1.4	
00032811008	07/15/2013	56488	12.6	
00032811009	07/16/2013	56489	1.0	
00032811010	08/13/2013	56517	5.4	
00032811011	08/15/2013	56519	6.7	

^aAt the start of the observation.

^bT1 is Transient 1; T2 is Transient 2; see §2.2.1 for details.

^cThe target fell in the stray light pattern of an unrelated source in Module B for this observation only. Hence for this observation B was omitted from the spectroscopic analysis.

Table 2: Phase-Coherent Timing Ephemerides for SGR J1745–2900

Parameter	Value
First Ephemeris	
MJD Range	56408–56450
Epoch	56415.42
Frequency ν (Hz)	0.2657067288(20)
Frequency Derivative $\dot{\nu}$ (Hz)	$-4.32(9) \times 10^{-13}$
Second Derivative $\ddot{\nu}$ (Hz/s)	$-8(1) \times 10^{-20}$
Period $P \equiv 1/\nu$ (s)	3.763547895(29)
Period Derivative, \dot{P}	$6.12(12) \times 10^{-12}$
Second Derivative, \ddot{P} (s^{-1})	$1.15(15) \times 10^{-18}$
RMS Residual (ms)	38
$\chi^2/\text{dof}/p^a$	113/86/0.03
Second Ephemeris	
MJD Range	56457–56519
Epoch	56513.00
Frequency ν (Hz)	0.265700350(9)
Frequency Derivative $\dot{\nu}$ (Hz)	$-9.77(10) \times 10^{-13}$
Second Derivative $\ddot{\nu}$ (Hz/s)	$-2.7(4) \times 10^{-20}$
Period $P \equiv 1/\nu$ (s)	3.76363824(13)
Period Derivative, \dot{P}	$1.385(15) \times 10^{-11}$
Second Derivative, \ddot{P} (s^{-1})	$3.9(6) \times 10^{-19}$
RMS Residual (ms)	51
$\chi^2/\text{dof}/p^a$	52/41/0.12

^a χ^2 , degrees of freedom, probability of chance occurrence.

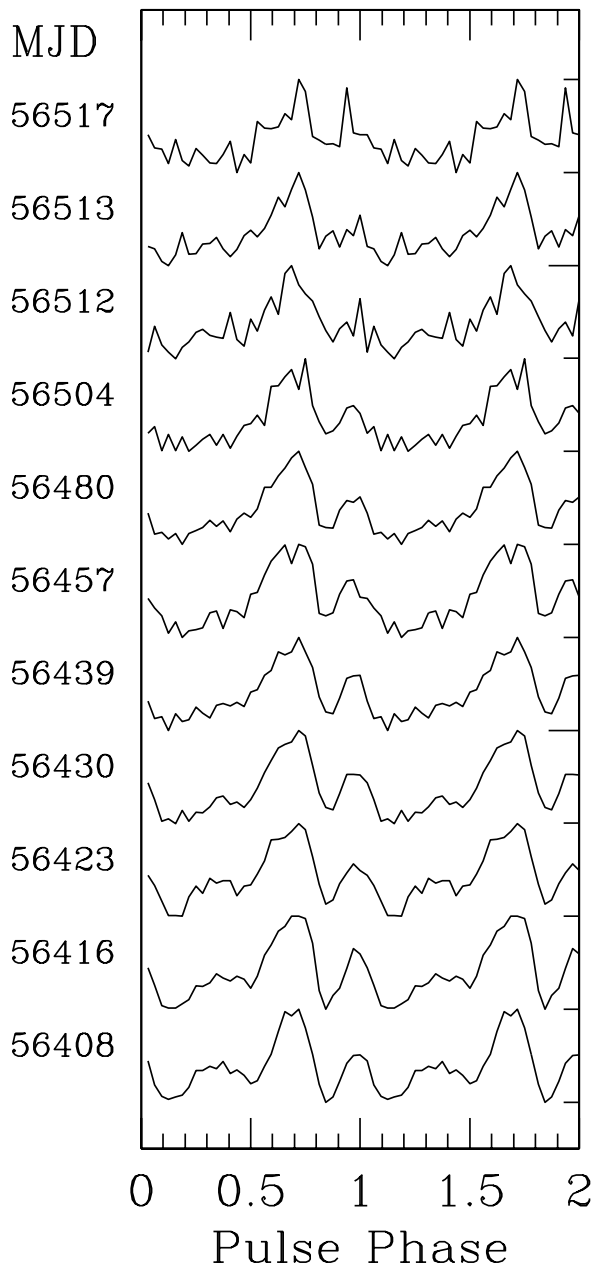


Fig. 1.— *NuSTAR* pulse profiles in the 3–10 keV band at the observing MJDs (see Table 1), aligned using the ephemerides presented in Table 2. Two cycles are shown for clarity. Note the gradual disappearance of the first of the three peaks seen in the MJD 56408 observation. Uncertainties on phase bins are omitted for clarity but are well represented by the off-pulse scatter.

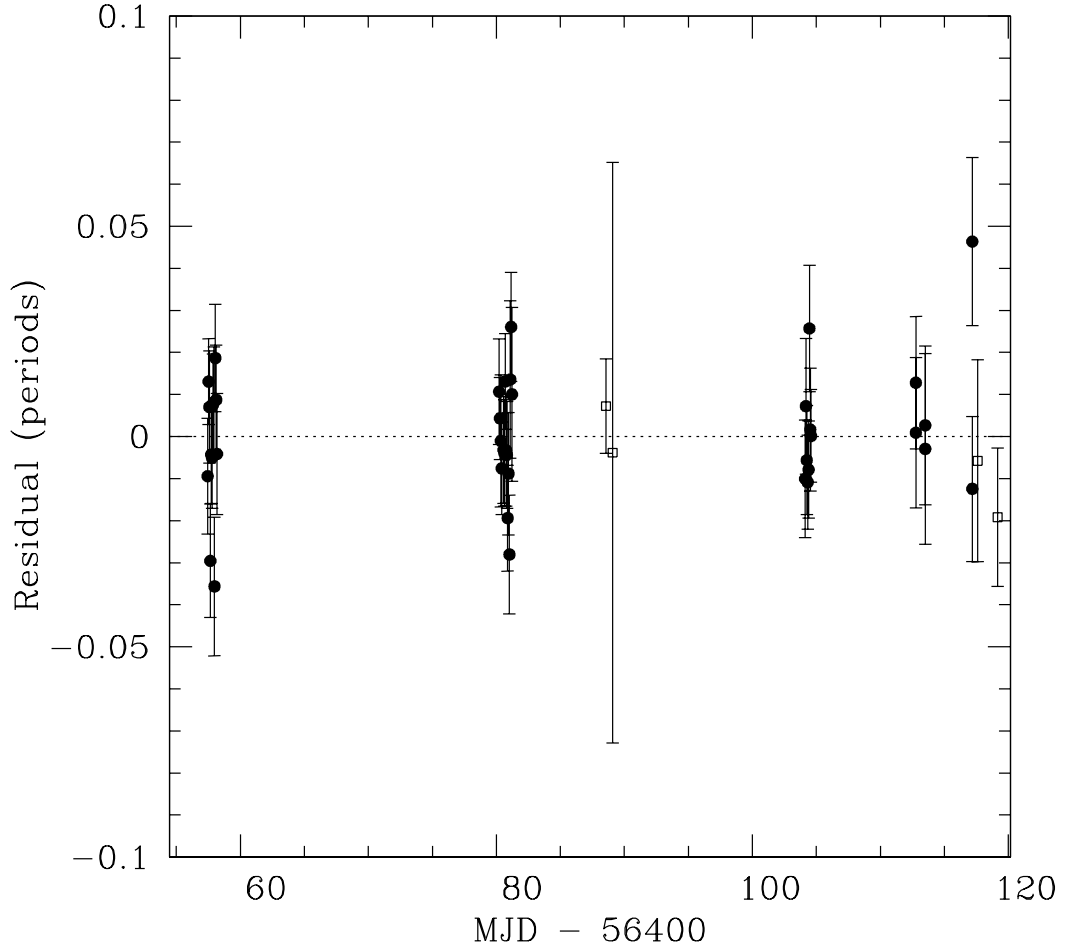


Fig. 2.— Residuals for the second phase-coherent timing solution shown in Table 2 for the appropriate MJD range. Filled circles are *NuSTAR* TOAs and empty squares are *Swift* TOAs.

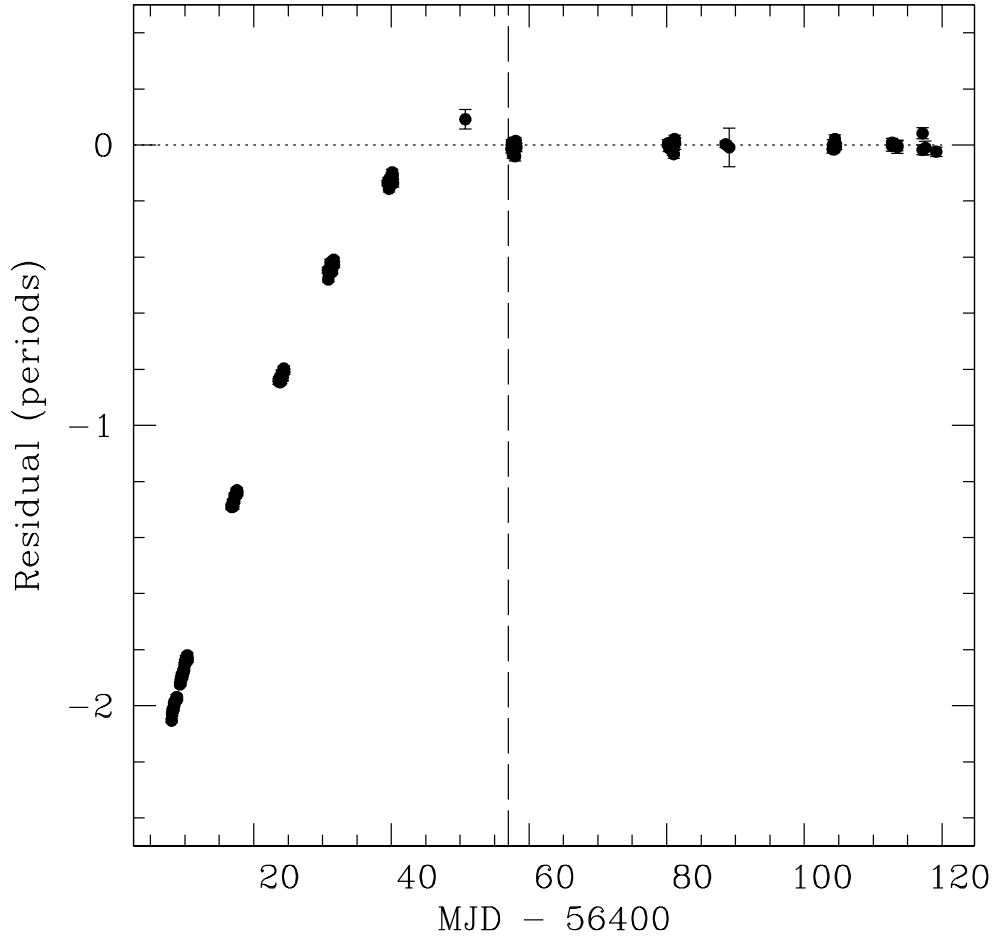


Fig. 3.— Attempt to extrapolate the second timing solution backward, showing growing phase deviations that demonstrate the change in ephemeris. The start of the 2nd ephemeris is indicated by the vertical dashed line.

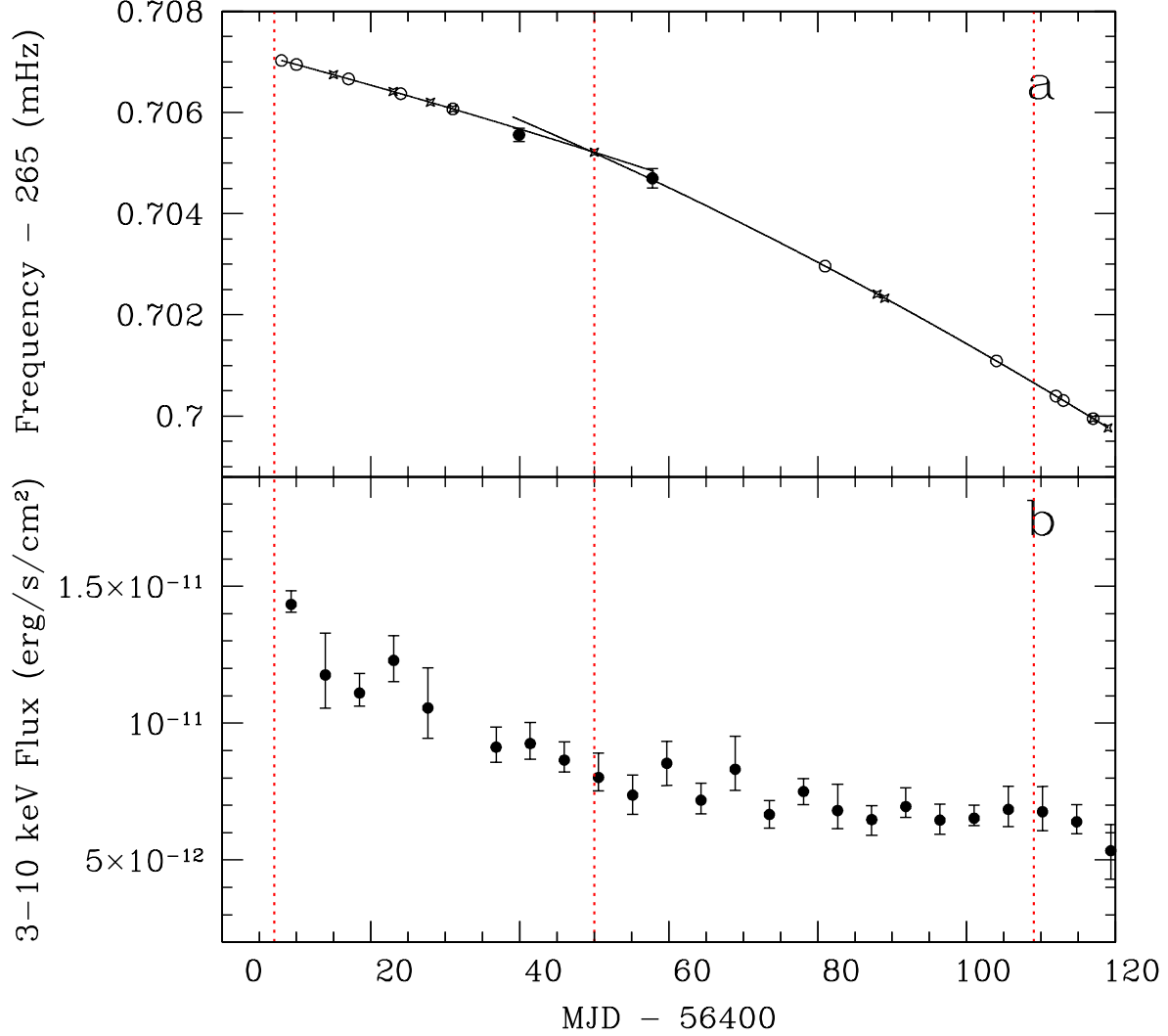


Fig. 4.— (a) Spin frequency versus time. The two solid lines represent the two different phase-coherent solutions discussed in §2.1 and presented in Table 2. Open circles and stars represent epochs of *NuSTAR* and WT-mode *Swift* XRT observations, respectively (see Table 1) with the frequencies calculated from the phase-coherent ephemerides. Note the overlap region between *NuSTAR* observations on MJDs 56439 and 56457 where both solutions can reasonably fit the phase data; locally calculated frequencies for those data sets are shown in solid circles along with error bars. The dotted vertical red lines indicate epochs of *Swift* BAT reported bursts on MJDs 56407 (April 25), 56450 (June 7) and 56509 (August 5). (b) Absorbed 3–10 keV flux versus time in 5-day averages from PC-mode *Swift* XRT observations. The gap in coverage near MJD 56430 was when nearby Transient 1 contaminated the magnetar fluxes (Dufour et al. 2013; Degenaar et al. 2013).

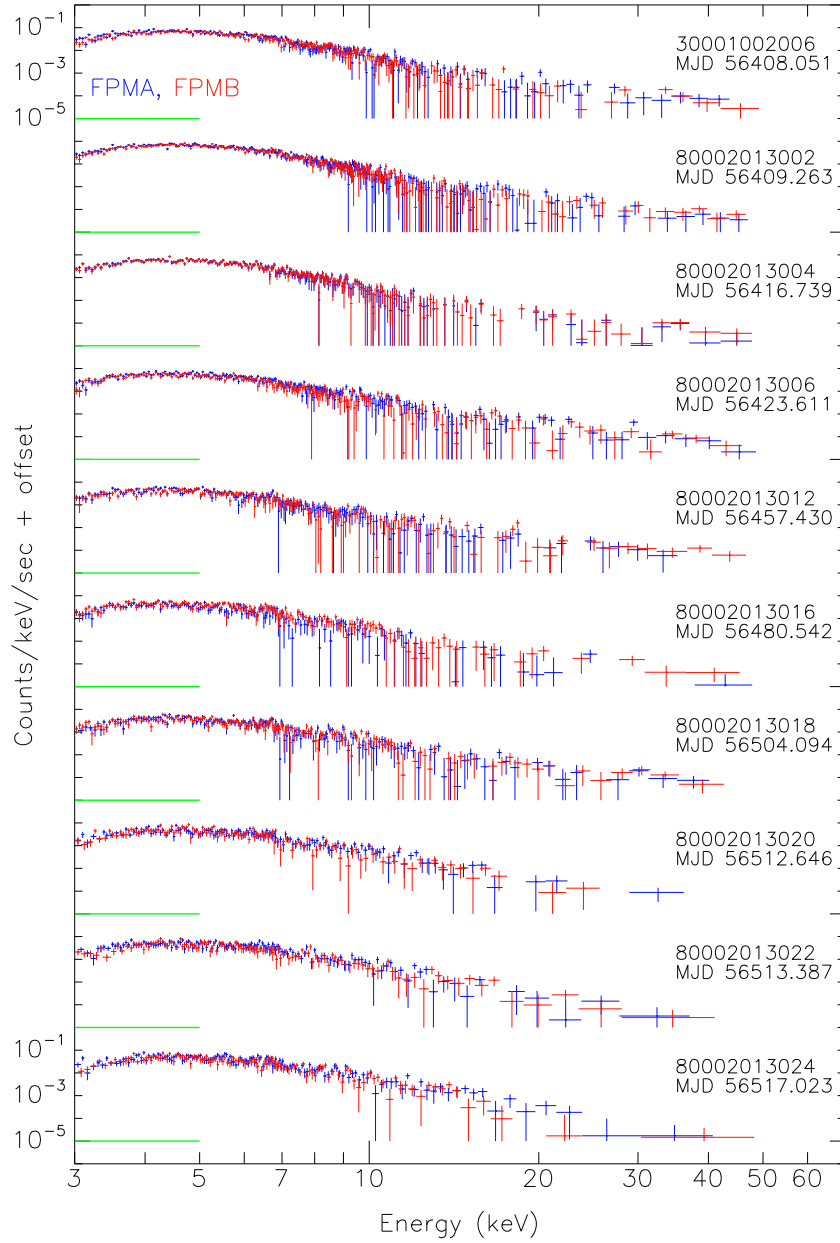


Fig. 5.— Spectra for all *NuSTAR* observations from earliest (top) to latest (bottom). FPMA is plotted in blue and FPMB is plotted in red. Spectra have been grouped to have a minimum of 20 counts per spectral bin.

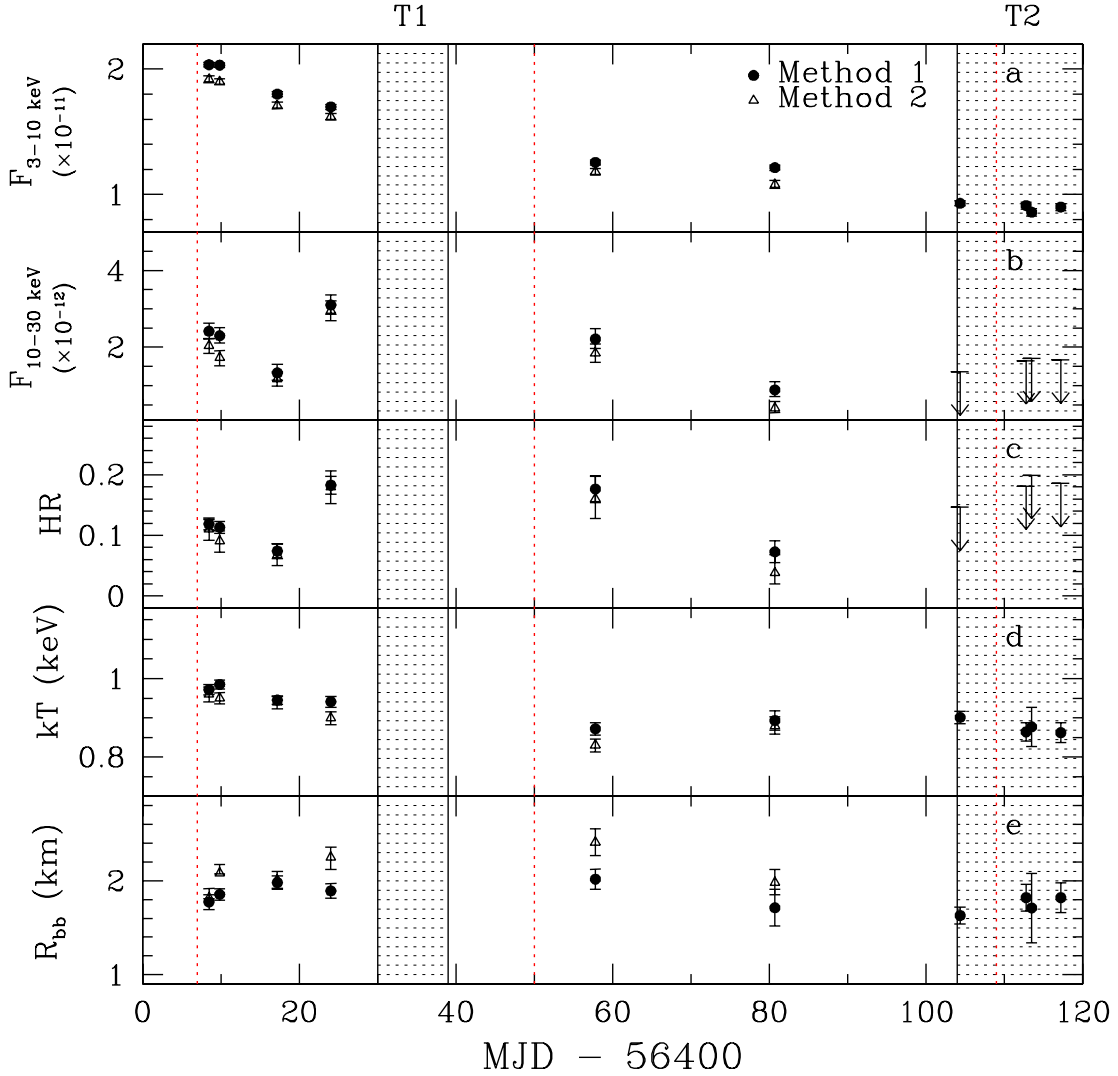


Fig. 6.— (a) Absorbed flux versus time in the 3–10 keV band in $\text{erg s}^{-1} \text{cm}^{-2}$, for Method 1 (solid circles) and Method 2 (open triangles). (b) Absorbed flux versus time in the 10–30 keV band in $\text{erg s}^{-1} \text{cm}^{-2}$, for Methods 1 and 2. Note that when Transient 2 is on, we present only upper limits for Method 1 and no values for Method 2. (c) Hardness ratio (defined as the ratio of the 10–30 keV to 3–10 keV absorbed fluxes), showing results from Methods 1 and 2. (d) Blackbody temperature kT for both Methods. (e) Blackbody radius R_{bb} in km for both Methods, obtained assuming a distance to the source of 8.0 kpc. All panels: hatched regions indicate epochs when Transient 1 (T1) and Transient 2 (T2) contaminated our *NuSTAR* data; data for SGR J1745–2900 when T1 was on were unusable for flux or spectroscopy. Vertical dotted red lines indicate epochs of X-ray bursts from the source direction.